



Piezo-phototronic effect enhanced polarization-sensitive photodetectors based on cation-mixed organic–inorganic perovskite nanowires

Laipan Zhu^{1,2,†}, Qingsong Lai^{1,2,†}, Wenchao Zhai^{1,2}, Baodong Chen^{1,2},
Zhong Lin Wang^{1,3,*}

¹ CAS Center for Excellence in Nanoscience, Beijing Key Laboratory of Micro-nano Energy and Sensor, Beijing Institute of Nanoenergy and Nanosystems, Chinese Academy of Sciences, Beijing 100083, PR China

² School of Nanoscience and Technology, University of Chinese Academy of Sciences, Beijing 100049, PR China

³ School of Material Science and Engineering, Georgia Institute of Technology, Atlanta, GA 30332, USA

Piezo-phototronic effect has been extensively investigated for the third generation semiconductor nanowires. Here, we present a demonstration that piezo-phototronic effect can even be applied to tune polarization-sensitive photodetectors based on cation-mixed organic–inorganic perovskite nanowires. A big anisotropic photoluminescence (PL) with linearly polarized light-excitation was found due to a strong spontaneous piezoelectric polarization besides the anisotropic crystal structure and morphology. The piezo-phototronic effect was utilized to tune the PL intensity, and an improved anisotropic PL ratio from 9.36 to 10.21 for linearly polarized light-excitation was obtained thanks to the modulation by piezo-potential. And a circularly polarization-sensitive PL characterized with circular dichroism ratio was also discovered, which was found to be modulated from 0.085 to 0.555 (with a 5.5-fold improvement) within the range of applied strain. The circular dichroism was resulted from the joint effects of the modulated Rashba spin–orbit coupling and the asymmetric carriers separation and recombination for right- and left-handed helicity due to the presence of effective piezo-potential. These findings not only reveal the promising optoelectronic applications of piezo-phototronic effect in perovskite-based polarization-sensitive photodetectors, but also illuminate fundamental understandings of their polarization properties of perovskite nanowires.

Introduction

In the field of traditional optical communication, the intensity, spectrum and spatial distribution of a light source are the three main parameters commonly used in our daily life. Polarization is another important information of light, hence the detection of polarization including polarization degree, polarization azimuth, ellipticity and circular polarization direction can greatly enrich the applications of light sensing [1–3]. Fabrication of anisotropic semiconductor structures, including anisotropic crystal

structure and anisotropic morphology, is essential for the development of linear-polarization photodetectors [1,4]. Semiconductor nanowires (NWs), with well-defined crystal and morphology anisotropy, have proven to be good candidates for linear polarization detection by means of light emission, absorption, and photoconductivity [1,4,5]. Semiconductor NWs especially with chip-level polarization sensitivity will have great potential in applications of future electronic circuits and optical chips. Over the past decade, halide perovskites have revealed excellent optical and optoelectronic properties, making them ideal candidates for the advancement of high-performance light sources, photodetectors and photovoltaic devices [6–10]. Recently, there are even reports on linear-polarization photodetectors based on

* Corresponding author.

E-mail address: Wang, Z.L. (zhong.wang@mse.gatech.edu)

† These authors contributed equally to this work.

organic–inorganic $(\text{CH}_3\text{NH}_3)\text{PbI}_3$ (abbreviated as MAPbI₃) and all-inorganic CsPbX_3 (X = Cl, Br, I) lead halide perovskite nanowires [11–13]. There are also experimental evidences that lead halide perovskites possess a big spin–orbit coupling (SOC) which makes them outstanding performances in optoelectronic applications [14–16].

The three way coupling between piezoelectric effect, semiconductor and photoexcitation creates three main significant research fields, namely, piezophotonics, piezotronics, and piezo-phototronics [17–19]. Piezotronic and piezo-phototronic effects are extensively existed in third generation semiconductors, transition-metal dichalcogenides, and perovskites [17,20–24]. Distinct from the first and the second generation semiconductors that are dominated by cubic crystal structure, such as Si, Ge and GaAs, the third generation semiconductors are dominated by non-cubic crystal structures such as Wurtzite and monoclinic etc, which lack of center symmetry. Therefore, piezoelectricity and piezotronic effect are the born characteristics of these semiconductors. The piezotronic effect involves utilizing the piezo-potential as a “gate” voltage to adjust/control the carrier transportation at the junction or interface. The piezo-phototronic effect is about the modulation of generation, separation, transportation or recombination of the photo-induced carriers at interfaces or junctions using the piezo-potential and piezoelectric charges. The piezo-phototronic effect has been used for many novel optoelectronic devices, for example, solar cells [25–27], LEDs [28,29], photosensors [24,30], spintronic devices [31,32].

In this work, we fabricated a cation-mixed organic–inorganic $\text{Cs}_x\text{MA}_{1-x}\text{PbI}_3$ perovskite nanowire, which revealed a better polarization sensitivity for not only linearly polarized light but also circularly polarized light. What's more important, apart from the anisotropic crystal structure and morphology, it was demonstrated for the first time that the piezo-potential can also be used effectively to tune the linear-polarization sensitivity as well as circular-polarization sensitivity. This work indicates that the piezo-phototronic effect can also work at one semiconductor interior besides the interfaces and junctions. This experimental work also confirms the presence of a big SOC in this type of perovskite nanowires, which is derived from the inner piezo-potential. These findings not only shed light on the promising optoelectronic applications of piezo-phototronic effect in perovskite-based polarization-sensitive photodetectors, but also reveal fundamental understandings of their polarization and spin-transport properties in perovskite nanowires.

Results and discussion

Herein, we have successfully synthesized well-defined organic–inorganic $\text{Cs}_x\text{MA}_{1-x}\text{PbI}_3$ perovskite nanowires, where inorganic cation Cs^+ is intentionally introduced to replace organic cation MA^+ in order to induce a certain degree of inner strain which turns out to be good for bringing in a spontaneous piezoelectric polarization in the nanowires. Fig. 1a shows the growing processes of the nanowires via a two-step solution process on glass/ITO substrate with the size of $1\text{ cm} \times 1\text{ cm}$. The as-prepared NWs has a wide light absorption spectrum ranging from ultraviolet (400 nm) to near infrared (825 nm) and shows

a good photoluminescence (PL) property with the peak intensity at about 740 nm, where the inset shows the scanning electron microscope (SEM) image of the as-fabricated black phase $\text{Cs}_x\text{MA}_{1-x}\text{PbI}_3$ nanowires with an average diameter of $2\text{ }\mu\text{m}$ (Figs. 1b and S1). The length of the nanowires to be used in following polarization-sensitive experiments is about $30\text{ }\mu\text{m}$. The time resolved PL (TRPL) decay kinetics with a 375 nm laser excitation in Fig. 1c shows that the PL decay time is about 10.7 ns, which is attributed to the free exciton recombination process [13]. The TRPL decay time is obtained from a glass/ITO/ $\text{Cs}_x\text{MA}_{1-x}\text{PbI}_3$ perovskites sample with the size of $1\text{ cm} \times 1\text{ cm}$, as shown in the inset of Fig. 1c. The powder X-ray diffraction (XRD) pattern in Figs. 1d and S2 (see Supplementary Information) indicates high crystalline quality of $\text{Cs}_x\text{MA}_{1-x}\text{PbI}_3$ perovskite nanowires with two phases including CsPbI_3 and MAPbI₃. The energy-dispersive X-ray (EDX) mapping in Fig. 1e shows the distinct presence of C, Cs, Pb and I elements, and the proportion of Cs and C is about 0.6/0.4 which means the proportion of cations Cs^+ and MA^+ is about 0.6/0.4. From the low-magnified transmission electron microscope (TEM) image (Fig. 1f), high resolved TEM (HRTEM) images and corresponding selected area electron diffraction (SAED) patterns with zone axis along $[0\ 1\ -2]$ (Fig. 1g) and $[0\ 0\ 1]$ (Fig. 1h), respectively, we can decide that the nanowires are grown along $[1\ 0\ 0]$ direction and they belong to anisotropic orthorhombic crystal structure with $a = 0.54\text{ nm}$, $b = 0.56\text{ nm}$ and $c = 0.96\text{ nm}$ (also see Supplementary Information Fig. S2).

Then, we transferred the as-fabricated nanowires onto a flexible polyethylene terephthalate/polymethylmethacrylate (PET/PMMA) substrate in order to applying axial strain on the NWs, where the NWs were partially buried into the PMMA (Figs. 2a; S4 and S5, Supplementary Information) for enhancing their mechanical endurance. A linearly polarized 532 nm laser was selected to irradiate vertically on the middle of the NW, where θ denotes the angle between the polarization direction of laser and the NW growth direction. We studied the polarization angle dependence of the PL spectra, which was mapped into a two-dimensional (2D) image, as shown in Fig. 2b. From Fig. 2b we can see that the PL intensity reaches to maximum values when the polarization is parallel to the axial direction of the NW, that is, the polarization is along $[100]$ direction, while it changes gradually to minimum values with the polarization changing to the direction perpendicular to $[1\ 0\ 0]$. Taking the peak wavelength 740 nm that corresponds to excitonic luminescence as a typical case, we analyzed the characteristics of the polarization property. From Figs. 2c and S6 in the Supplementary Information, we can see that the PL intensity corresponding to 740 nm and $\theta = 0^\circ$ was increased dramatically with the increase of light power and began to saturate when the power surpasses 1.5 mW. From Fig. 2d, an obvious anisotropic PL intensity was found, with an anisotropic ratio $\rho = I_{\parallel}/I_{\perp}$ reaching up to 9.54, where I_{\parallel} and I_{\perp} denote the PL intensity for $\theta = 0^\circ$ and $\theta = 90^\circ$, respectively. It is much higher than many polarization anisotropy using photocurrent detection method, such as CsPbI_3 nanowires ($\rho = 2.68$) [12], MAPbI₃ nanowires ($\rho = 1.3$) [11], InP nanowires ($\rho = 0.96$) [1], and CdSe nanowires ($\rho = 0.75$) [4]. The origin of this high polarization sensitivity results from the selective absorption because of the anisotropic morphology, the highly anisotropic crystal

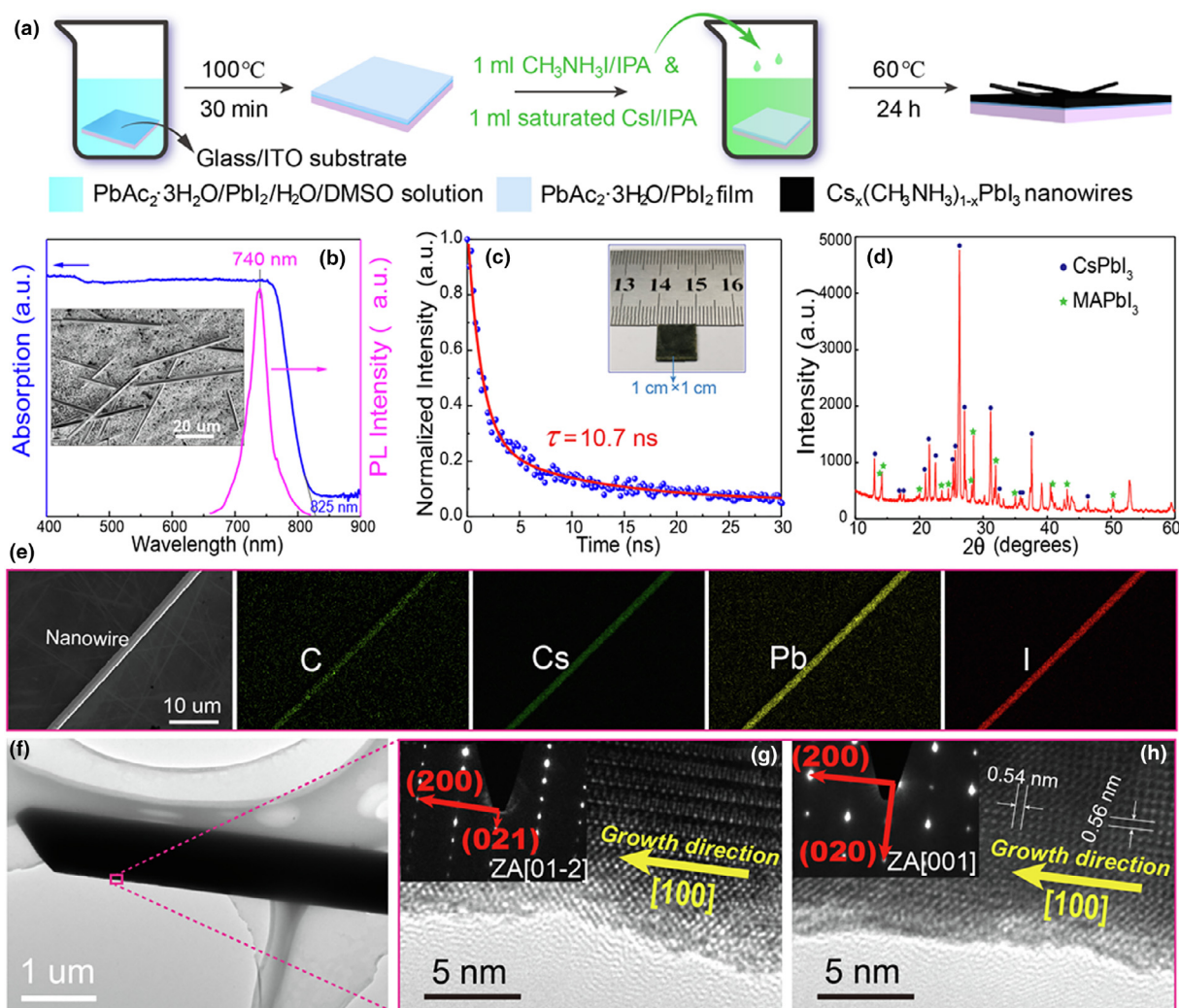


FIGURE 1

Fabrication and characterization of the cation-mixed perovskite nanowires. (a) Fabrication of organic–inorganic hybrid perovskite nanowires. (b) Absorption and PL spectra of the fabricated samples, where the inset denotes the SEM image of the nanowires. (c) TRPL decay kinetics after a 375 nm pulse laser excitation, where the inset shows the optical image of the as-fabricated perovskite nanowires on glass/ITO substrate with the size of 1 cm × 1 cm. (d) Powder X-ray diffraction of the fabricated samples. (e) EDX mapping corresponding to one of the fabricated NWs. (f–h) Low-magnified TEM image (f), HRTEM images and corresponding SAED patterns with zone axis along [0 1 –2] (g) and [0 0 1] (h), respectively.

structure of the NWs, and the strong spontaneous piezoelectric polarization of mixed-cations in the NW growth direction due to the large inner strain as the introduction of Cs⁺. Actually, piezoelectric properties in pure (one type of cation) organic–inorganic perovskites have already been reported by many former studies due to the polarization of cations [23,24,33,34].

We also studied the strain dependence of the polarization detection. The diagrams of the nanowire under a compressive strain were shown in Fig. 3a when an upward bending was applied on the substrate, where four typical cases were considered with different excitation polarizations, i.e., linearly polarized light with $\theta = 0^\circ$ and $\theta = 90^\circ$ as well as circularly polarized light with right- and left-handed helicity. The variation of the peak wavelength (740 nm) due to the change of strain can be regardless, as shown in Figs. 3b and S7 in the Supplementary Information. Piezoresistive effect usually changes the energy bandgap, as a result it will make the PL peak moving obviously.

The energy bandgap kept almost unchanged within the range of applied strain, making a negligible peak variation, which proved that the influence of piezoresistive effect on the modulation of PL intensity might be ignored. In the insets of Fig. 3b, we sketched the way how to apply strain on the nanowire. The applied strain on the nanowire along [100] direction can be expressed as $\varepsilon = \frac{d \sin \alpha}{L} \times 100\%$, where d , L and α are the thickness of the flexible substrate, the distance between the two holders used for fixing the two end of the substrate, and the bending angle of the substrate, respectively. Fig. 3c shows the strain dependence of PL intensity and anisotropic ratio with $\theta = 0^\circ$ and $\theta = 90^\circ$ when linearly polarized light was applied (abstracted from Fig. S7a,b). The PL intensities for this two cases were both increased with the strain ranging from -0.31% to $+0.31\%$, but the value of the case for $\theta = 0^\circ$ was much bigger by an order of magnitude than that for $\theta = 90^\circ$. The strength of this anisotropy was characterized by anisotropic ratio ρ . We can see that the ani-

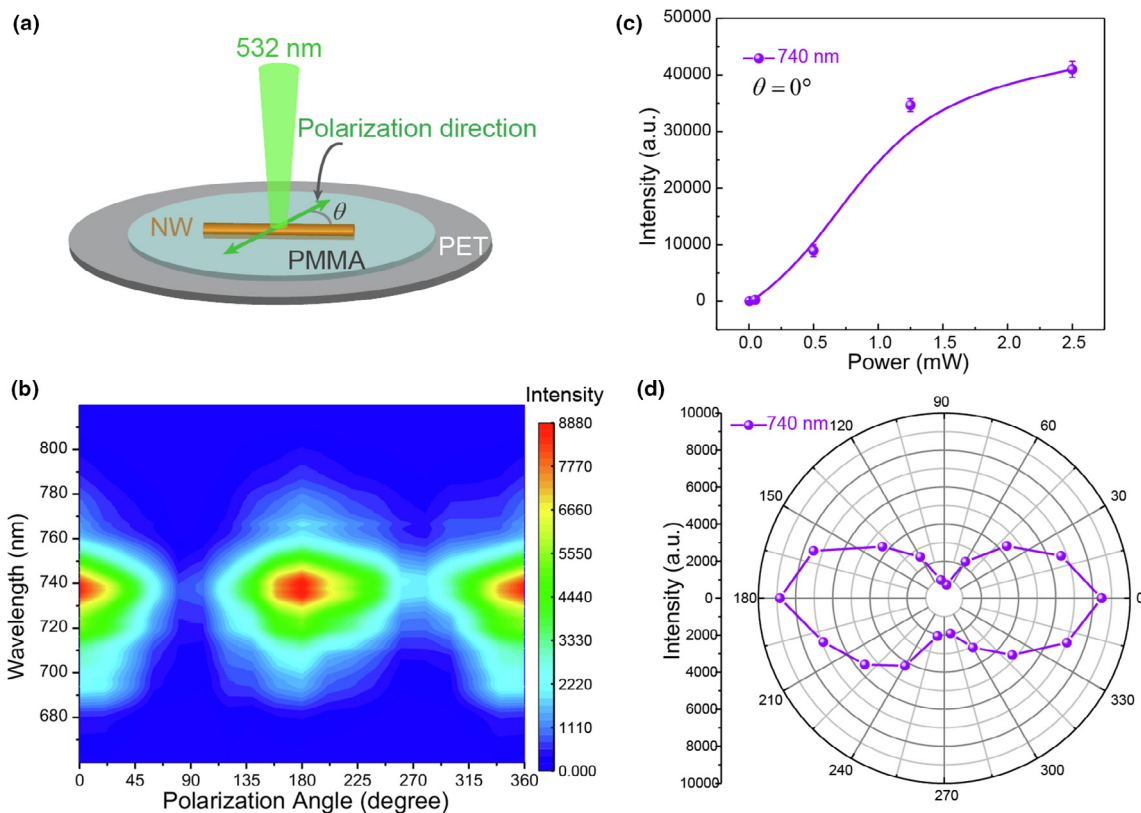


FIGURE 2

Polarization-sensitive photodetector for linearly polarized light. (a) Schematic diagram of a NW lying on a flexible PET/PMMA substrate and irradiated with a linearly polarized 532 nm laser, where θ denotes the angle between the polarization direction of laser and the NW growth direction. (b) PL intensity mapping as a function of polarization angle and wavelength with a light power of 0.5 mW. (c) PL intensity at 740 nm as a function of laser power when θ is set to be 0° . (d) Polar coordinate curve of PL intensity at 740 nm as a function polarization angle.

sotropic ratio ρ was increased rapidly from 9.54 to 10.21 with the increase of compressive strain, while it was reduced gradually from 9.54 to 9.36 with the increase of tensile strain. Interestingly, the PL intensities were also different for right- and left-handed circularly polarized light excitation, respectively, as shown in Figs. 3d and S7c,d in the Supplementary Information. Generally speaking, the PL intensities were all increased almost linearly with the strain ranging linearly from -0.31% to $+0.31\%$. The PL intensity for left-handed helicity was much larger than that for right-handed helicity. A circular dichroism ratio expressed as $\beta = (I_{\sigma^-} - I_{\sigma^+}) / (I_{\sigma^-} + I_{\sigma^+})$ was used to characterize the anisotropy of circularly polarized light, which was closely related with the spin-orbit coupling in the nanowire [35,36]. This circular dichroism ratio was decreased linearly with the increase of tensile strain and increased linearly with the increase of compressive strain, which meant that the inner spin-orbit coupling was changed due to the induced piezo-potential under the applied strain. In the next part, we proposed a possible physical mechanism to understand these experimental phenomena.

If no external strain was applied on the nanowire, there was still spontaneous piezoelectric polarization along the axial direction ([1 0 0] direction) of the nanowire, which might derive from the polarized redistribution of mixed-cations due to the residual strain (see Fig. 4a). The as-fabricated nanowires belonged to high-quality anisotropic orthorhombic structure, and the lattice con-

stant in [1 0 0] direction was 0.54 nm. The PL intensity was resulted from the recombination of free excitons (electron-hole pairs binding with coulomb forces), whose recombination lifetime has been measured to be 10.7 ns from the TRPL measurement (Fig. 1c). The piezo-potential inside the nanowire tuned the separation and recombination of the photo-induced carriers. When a compressive strain was applied on the axial direction of the nanowire, an external piezo-potential was induced, whose direction was inferred to be the same as the direction of spontaneous piezoelectric polarization (Fig. 4b). The increased piezoelectric field enhanced the separation of electron-hole pairs, hence reduced the recombination of carriers (or excitons), as a result the PL intensities for all the four cases in Fig. 3a were decreased. On the contrary, when a tensile strain was applied on the axial direction of the nanowire, the external piezo-potential offset the spontaneous piezo-potential, thus the separation of electron-hole pairs was weakened and the recombination of excitons was increased, finally the PL intensities for all the four cases in Fig. 3a were increased (see Fig. 4c).

From Fig. 3c, we can see that the stronger the effective piezo-potential was, the stronger the anisotropy ratio was. Piezo-potential was enhanced under compressive strain but reduced under tensile strain. The variation of anisotropy ratio under tensile strain was much weaker than that for compressive strain, which was due to the increased anisotropy of crystal structure

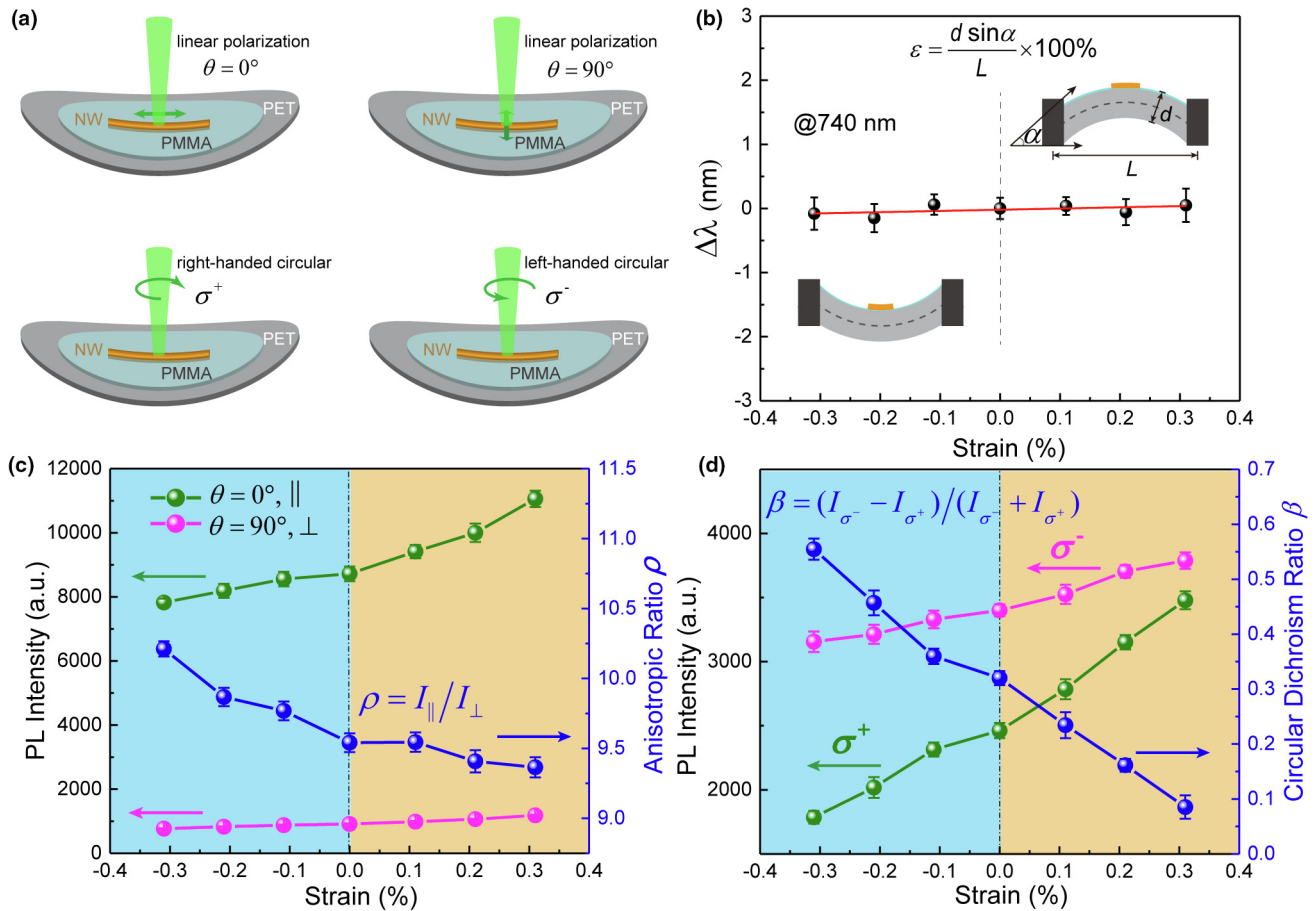


FIGURE 3

Polarization-sensitive detectors under the influence of external strain. (a) The upper two insets illustrate excitation using linearly polarized light with $\theta = 0^\circ$ and $\theta = 90^\circ$, respectively. The bottom two insets illustrate excitation using right- and left-handed circularly polarized light, respectively. All the cases are under a compressive strain. (b) The movement of the PL peak position (corresponding to 740 nm) under different strains, where the insets sketch the way how to apply a strain on the nanowire and the calculation of the applied strain. (c) Strain dependence of PL intensity and anisotropic ratio with $\theta = 0^\circ$ and $\theta = 90^\circ$, respectively. (d) Strain dependence of PL intensity and circular dichroism ratio with excitation of right- and left-handed circularly polarized light, respectively.

and morphology under tensile strain. So the contribution for the anisotropy ratio from the increased anisotropy of crystal structure and morphology offset partially due to the reduced piezo-potential when a tensile strain was applied. As a result, an increased anisotropic ratio with increased compressive strain and a decreased anisotropic ratio with increased tensile strain were found, as shown in Fig. 3c. In other words, the piezo-potential could be used effectively to tune the PL intensity as well as the anisotropic ratio. The piezo-potential along [100] direction will introduce a Rashba term in Hamiltonian: [35,37,38] $H = \chi_{xx}\sigma_x k_x$, where χ_{xx} is the second-order pseudotensor depends on the symmetry and the coordinate system used, σ_x is the Pauli matrices, and k_x is the momentum vector along x direction. This Rashba spin-orbit coupling resulted in a spin splitting in the energy band, as shown in Fig. 4d. The right-handed polarized light excited spin polarized electrons and holes, which relaxed to the bottom of conduction band and the top of valence band, respectively, due to inelastic phonon scattering, and then went through an indirect radiative recombination [39,40]. The indirect and spin-forbidden recombi-

nation path had a significantly slower transition rate due to the mismatch of momentum and spin. The radiative recombination was constrained with enhanced spin-splitting of energy band when a compressive strain was applied (Fig. 4e). While the radiative recombination was increased with reduced spin-splitting of energy band when a tensile strain was applied (Fig. 4f). Thus the changes of spin-splitting of energy band could also result in the changes of PL intensity in Fig. 3d besides the tilted energy bands in Fig. 4a,c. The circular dichroism ratio was increased when a compressive strain was applied as illustrated in Fig. 3d, which was attributed to the different separation and recombination rates for right- and left-handed helicity excitation under the influence of effective piezoelectric field (or piezo-potential). The piezoelectric field played two important roles, inducing spin-splitting of energy band and tuning the separation and recombination of carriers for right- and left-handed helicity. As shown in Fig. 4g, if there is no effective piezoelectric field ($E = 0$), the PL intensity should be the same for right- and left-handed helicity excitation. When there was a smaller effective piezoelectric field ($E > 0$), the field would promote the radiative recombination of

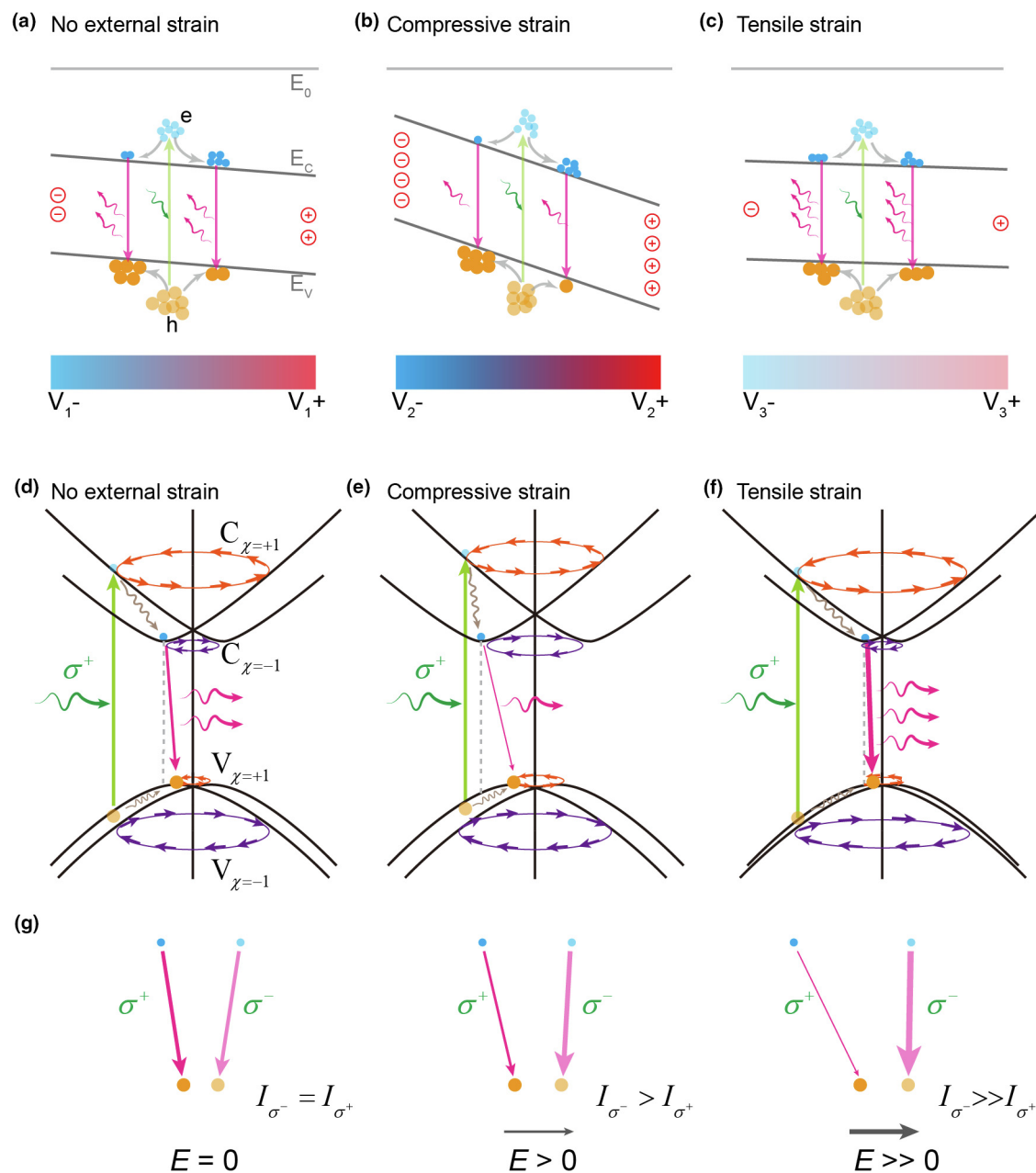


FIGURE 4

Proposed mechanisms of the piezo-phototronic effect tuned polarization-sensitive photodetectors. (a) Schematic energy band image with spontaneous piezoelectric polarization even without external strain. (b) Schematic energy band image with enhanced piezoelectric polarization under a compressive strain. (c) Schematic energy band image with reduced piezoelectric polarization under a tensile strain. (d–f) Diagrams of Rashba spin-splitting bands and the electron transport paths with no strain (d), compressive strain (e) and tensile strain (f), where $C_{\chi=+1}$ ($V_{\chi=+1}$) and $C_{\chi=-1}$ ($V_{\chi=-1}$) represent “counter-clockwise” and “clockwise” spin texture for conduction (valence) band electrons (holes), respectively. (g) Schematic diagrams denoting the modulation of circular dichroism via the effective piezoelectric field.

carriers excited by left-handed polarized light due to the reduced momentum mismatch, while suppressed the recombination of carriers excited by right-handed polarized light. When the effective piezoelectric field was further increased ($E \gg 0$), the difference of radiative recombination for right- and left-handed helicity excitation would be further increased. As a result, we found an increased and decreased circular dichroism ratio for the increase of compressive and tensile strain, respectively.

Conclusions

Linear and circular polarization-sensitive photodetectors based on cation-mixed organic–inorganic perovskite nanowires was fabricated. We found a big anisotropic PL with linearly polarized light-excitation, which was mainly derived from the strong spontaneous piezoelectric polarization in nanowires apart from the anisotropic crystal structure and morphology. Piezo-phototronic effect was utilized to tune the PL intensity, that is,

the compressive strain was demonstrated to reduce the PL intensity due to an increased piezo-potential while the tensile strain was on the contrary due to the weakened piezo-potential. An improved anisotropic PL ratio from 9.36 to 10.21 for excitation of linearly polarized light was confirmed when the strain was changed linearly from +0.31% tensile strain to -0.31% compressive strain. And we also discovered different PL intensity even for the excitation of right- and left-handed circularly polarized light, which resulted from the presence of Rashba spin-orbit coupling due to the strong spontaneous piezoelectric polarization along the axial direction of the nanowires. A circular dichroism ratio was found to be modulated from 0.085 to 0.555 (with a 5.5-fold improvement) when the strain was ranged from +0.31% tensile strain to -0.31% compressive strain, which was derived from not only the asymmetry tuning of carrier separation and recombination for right- and left-handed circular light excitation but also the modulation of Rashba spin-splitting of energy band due to the effective piezo-potential. These findings not only reveal the promising optoelectronic applications of piezophototronic effect in perovskite-based polarization-sensitive photodetectors, but also illuminate fundamental understandings of their polarization properties of perovskite nanowires.

Experimental section

Device fabrication

The glass/ITO was cleaned in turn by acetone, alcohol, and deionized water in ultrasonic cleaners for 15 min. To fabricate $\text{Cs}_x(\text{CH}_3\text{NH}_3)_{1-x}\text{PbI}_3$ nanowires, we firstly dropped 150 μL 24 mg/mL $\text{PbAc}_2 \cdot 3\text{H}_2\text{O}/\text{H}_2\text{O}$ and DMSO (v:v = 2:1) solution and 50 μL PbI_2 saturated aqueous solution to the ITO respectively to form a $\text{PbAc}_2 \cdot 3\text{H}_2\text{O}/\text{PbI}_2$ thin film and dried the thin film for 30 min at 65 °C to evaporate off the solvent. We then immersed the thin film formed on glass/ITO in 1 mL 40 mg/mL $\text{CH}_3\text{NH}_3\text{I}$ and 1 mL saturated CsI isopropanol solution for ~24 h at 60 °C to grow the single-crystal NWs. The NWs were then transferred from the glass/ITO substrate using a heat-release tape of $10 \times 10 \text{ mm}^2$ size at room temperature. Next, a 220 nm PMMA was spin-coated onto the circular PET substrate with a diameter of 3 cm and then the PET/PMMA substrate was heated at 120 °C. The heat-release tape with NWs was pressed vertically on the PET/PMMA substrate and kept for 1 min. Since 120 °C was within both the range of PMMA's glass transition temperature and the temperature range of releasing adhesiveness of the heat-release tape, the NWs were transferred to PMMA with them partially buried into the PMMA. After a natural cooling from 120 °C to room temperature, the NWs were fastened on the PET/PMMA substrate.

Characterization and measurement

The absorption spectra was tested by using a UV-vis-NIR spectrophotometer (SHIMADZU UV3600). The polarization-sensitive PL spectra were obtained by using a confocal microprobe Raman spectroscopy (HORIBA/LabRAM HR Evolution) with the laser spot of 2 μm , whose schematic experimental setup and optical path of the measurement are shown in Fig. S8 (Supplementary Information). The TRPL decay kinetics with a 375 nm pulsed laser as light source was measured using a full-function steady-state/transient fluorescence spectrometer

(FLS980-S2S2-stm). The XRD pattern was acquired using a PANalytical X'Pert³ Powder X-ray diffractometer with Cu $\kappa\alpha$ source ($\lambda = 0.154 \text{ nm}$). The microscopic morphological characterization and EDX mapping were taken from a field-emission scanning electron microscope (Nova NanoSEM 450). The low-magnified TEM, HRTEM and corresponding SAED patterns were obtained with a transmission electron microscope (FEI Tecnai G2 F20). Two 3-dimensional positioning systems were used to bend the flexible substrate.

CRedit authorship contribution statement

Laipan Zhu: Conceptualization, Methodology, Data curation, Investigation, Writing - original draft, Writing - review & editing. **Qingsong Lai:** Methodology, Data curation, Investigation, Writing - original draft, Writing - review & editing. **Wenchao Zhai:** Visualization, Investigation. **Baodong Chen:** Visualization, Investigation. **Zhong Lin Wang:** Conceptualization, Formal analysis, Supervision, Writing - original draft, Writing - review & editing.

Acknowledgements

This research was supported by the National Natural Science Foundation of China (Grant No. 11704032, 51432005, 5151101243, 51561145021), National Key R & D Project from Minister of Science and Technology (2016YFA0202704), Beijing Municipal Science & Technology Commission (Z171100000317001, Z171100002017017, Y3993113DF). We also thank professor Yong Ding at Georgia Institute of Technology for the helpful discussion of TEM.

Appendix A. Supplementary data

Supplementary data to this article can be found online at <https://doi.org/10.1016/j.mattod.2020.02.018>.

References

- [1] J. Wang et al., *Science* 293 (5534) (2001) 1455.
- [2] J.S. Tyo et al., *Appl. Opt.* 45 (22) (2006) 5453.
- [3] Y. Ge et al., *J. Inf. Display* (2019), <https://doi.org/10.1080/15980316.2019.1654550>.
- [4] A. Singh et al., *Nano Lett.* 7 (10) (2007) 2999.
- [5] Z. Fan et al., *Appl. Phys. Lett.* 85 (25) (2004) 6128.
- [6] Z. Wu et al., *Adv. Optical Mater.* 6 (22) (2018) 1800674.
- [7] Z. Liu et al., *ACS Nano* 12 (6) (2018) 5923.
- [8] H. Wang, D.H. Kim, *Chem. Soc. Rev.* 46 (17) (2017) 5204.
- [9] Y. Cao et al., *Nature* 562 (7726) (2018) 249.
- [10] M.A. Green et al., *Nat. Photonics* 8 (2014) 506.
- [11] L. Gao et al., *Nano Lett.* 16 (12) (2016) 7446.
- [12] Y. Zhou et al., *Adv. Optical Mater.* 6 (22) (2018) 1800679.
- [13] Y. Gao et al., *Adv. Mater.* 30 (31) (2018) 1801805.
- [14] J. Wang et al., *Nat. Commun.* 10 (1) (2019) 129.
- [15] M. Kepenekian, J. Even, *J. Phys. Chem. Lett.* 8 (14) (2017) 3362.
- [16] J. Li, P.M. Haney, *Appl. Phys. Lett.* 109 (19) (2016) 193903.
- [17] Z.L. Wang et al., *MRS Bull.* 43 (12) (2018) 922.
- [18] Z.L. Wang, *Nano Today* 5 (6) (2010) 540.
- [19] Z.L. Wang, *Mater. Today* 10 (5) (2007) 20.
- [20] C. Pan et al., *Chem. Rev.* 119 (15) (2019) 9303.
- [21] P. Lin et al., *Adv. Funct. Mater.* (2018) 1802849.
- [22] J. Kou et al., *J. Phys. D Appl. Phys.* 51 (49) (2018) 493002.
- [23] L. Leppert et al., *J. Phys. Chem. Lett.* 7 (18) (2016) 3683.
- [24] Q. Lai et al., *ACS Nano* 12 (10) (2018) 10501.
- [25] L. Zhu, Z.L. Wang, *Adv. Funct. Mater.* 29 (41) (2018) 1808214.
- [26] L. Zhu et al., *Adv. Sci.* 4 (1) (2017) 1600185.
- [27] L. Zhu et al., *ACS Nano* 11 (2) (2017) 1894.

- [28] M. Chen et al., *ACS Nano* 10 (6) (2016) 6074.
- [29] C. Pan et al., *Nat. Photonics* 7 (9) (2013) 752.
- [30] Y. Dai et al., *ACS Nano* 11 (7) (2017) 7118.
- [31] L. Zhu, Z.L. Wang, *J. Phys. D Appl. Phys.* 52 (34) (2019) 343001.
- [32] L. Zhu et al., *ACS Nano* 12 (2) (2018) 1811.
- [33] V. Jella et al., *Nano Energy* 57 (2019) 74.
- [34] Y.-J. Kim et al., *J. Mater. Chem. A* 4 (3) (2016) 756.
- [35] J.L. Yu et al., *Appl. Phys. Lett.* 102 (7) (2013) 072404.
- [36] E.W. Bogaart et al., *Phys. Rev. B* 74 (15) (2006) 153307.
- [37] S. Ganichev, W. Prettl, *J. Phys. Condens. Mater.* 15 (2003) R935.
- [38] S. Ganichev et al., *Nature* 417 (6885) (2002) 153.
- [39] F. Zheng et al., *Nano Lett.* 15 (12) (2015) 7794.
- [40] Y. Ping, J.Z. Zhang, *J. Phys. Chem. Lett.* 9 (20) (2018) 6103.